Cautionary note on use of focused ion beam sectioning as technique for characterising oxidation damage in Ni based superalloys

Cruchley, S.; Sun, Jifeng; Taylor, Mary; Evans, Hugh; Bowen, P.; Sumner, J.; Nicholls, J. R.; Simms, N. J.; Shollock, B. A.; Chater, R. J.; Foss, B. J.; Hardy, M. C.; Stekovic, S.

DOI:
10.1179/0960340913Z.0000000004

This is the Author's copy of an Accepted Manuscript of an article published by Taylor & Francis in Materials at High Temperatures on 17th February 2014, available online:
http://www.tandfonline.com/doi/abs/10.1179/0960340913Z.0000000004

Cautionary Note on the use of Focussed Ion Beam (FIB) Sectioning as a Technique for Characterising Oxidation Damage in Ni-based Superalloys

S. Cruchley[1], Jifeng Sun[1], M.P. Taylor[1] , H.E. Evans[1], P. Bowen[1], J. Sumner[2], J.R. Nicholls[2], N.J. Simms[2], B.A. Shollock[3], R.J. Chater[3] , B.J. Foss[3] , M.C. Hardy[4] and S. Stekovic[5].

[1]School of Metallurgy and Materials, University of Birmingham, Birmingham, B15 2TT, UK

[2]School of Applied Sciences, Cranfield University, Cranfield, Bedfordshire, MK43 0AL, UK

[3]Department of Materials, Imperial College, London, SW7 2AZ, UK

[4]Rolls-Royce plc., Derby, DE24 8BJ, UK

[5]Formerly at Rolls-Royce plc., now at Linköping University, 581 83 Linköping, Sweden

Keywords: Focussed Ion Beam, Ni-based Superalloy, Oxidation, Internal Oxidation, Voids, SIMS.

ABSTRACT

Previous observations on Ni-based superalloys, obtained through the use of focussed ion beam (FIB) sample preparation and imaging, have reported the presence of sub-surface voids after oxidation. In this present study, oxidised specimens of the Ni-based superalloy, RR1000, were subjected to conventional sample preparation as well as both dual and single beam FIB preparation, with the aim of re-examining the previous observations of sub-surface void formation. It is clear from FIB preparations that features previously interpreted as networks of voids have been demonstrated to be internal oxides by varying the sample tilt angles and imaging signal using either secondary electrons (SE) or secondary ions (SI). Conventional preparation methods illustrate the presence of sub-surface alumina intrusions and the absence of voids, supporting previous evidence. The positive identification of voids and oxides by FIB can be complex and prone to misinterpretation and thus the use of several imaging conditions and tilt angles must be used, along with conventional preparation methods, to confirm or refute the presence of 'voids' underneath oxides.

INTRODUCTION

It is well established that chromia-forming Ni-Cr-Al alloys can form sub-surface alumina intrusions during oxidation exposure. Such intrusions are features of pure ternary alloy systems [1] as well as advanced Ni-based superalloys [1-5]. Recently, however, it has been claimed [6-8] that sub-surface voids occur as a consequence of oxidation and these may or may not be associated with alumina intrusions (Figure 1). These observations were made using single-beam focussed ion beam (FIB)

techniques [6-8] and conflict with observations of simple alumina intrusions, obtained using conventional preparation techniques [2-3, 5]. FIB sample preparation is now commonly used to examine cross-sections to establish the near-surface microstructure, without time-consuming metallographic procedures and is particularly advantageous for samples with brittle surface layers such as oxides.

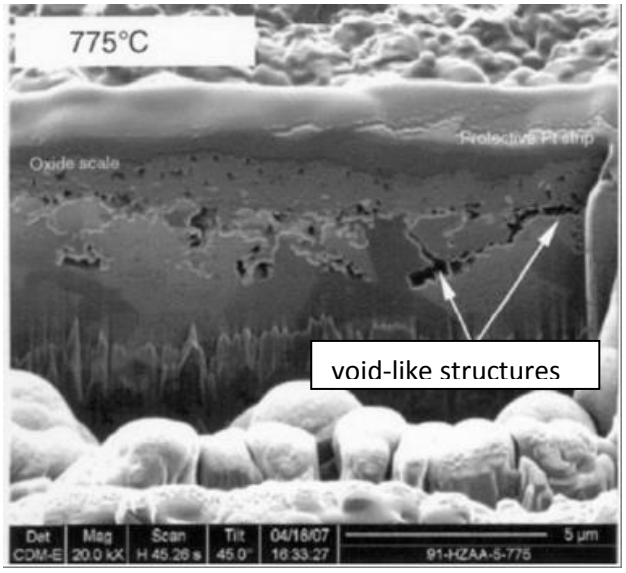

Figure 1. Image taken from Encinas-Oropesa et al. showing possible grain boundary voids underneath the oxide scale in RR1000. FIB section on a sample from an isothermal oxidation exposure at 775ºC for 200 hours [7].

The formation of voids under a growing oxide layer is an established phenomenon in metallic alloys and has been variously attributed to vacancy injection [9], dissociation of Cr-rich carbides [10], differing diffusion rates of elements within the alloy [11] or the internal oxidation of carbides or carbon in solution to form CO_2/CO gas bubbles [12]. Thermodynamic calculations [13, 14] show that this last mechanism will not occur under a chromia or alumina layer and, thus, would not be expected for most high-temperature alloys and particularly for the chromia-forming Ni-based superalloy (RR1000) to be considered here. The first two mechanisms, of vacancy injection and particle dissociation, are feasible in principle. The purpose of this note is to re-examine previous observations of sub-surface void formation in this alloy through a comparison of FIB and conventional preparation techniques to assess whether voids can be produced as an artefact of sample preparation, sample oxidation and image interpretation.

EXPERIMENTAL APPROACH AND RESULTS

Materials

The nominal compositions of two batches of the Ni-based superalloy, RR1000, (with and without Si) are given in Table I. The alloy was available in four conditions: CG RR1000, FG RR1000, FG RR1000 + 0.5 wt.% Si and shot-peened (SP) CG RR1000. The coarse-grained (CG) and fine-grained (FG) variant of the alloy had grain sizes of 30-50 μm and 4-6 μm, respectively. Shot-peening was performed using the following parameters of shot type, intensity and coverage: 110H, 6-8A and 200%, respectively.

Table 1: Nominal composition of RR1000, with and without Si, in both atomic and weight %.

Alloy		Ni	Co	Cr	Mo	Ti	Al	Ta	Hf	Zr	C	B	Si
RR1000	Wt. %	bal.	18.5	15.0	5.0	3.6	3.0	2.0	0.50	0.06	0.02	0.03	--
	At. %	bal.	17.9	16.5	3.0	4.3	6.4	0.63	0.16	0.04	0.14	0.10	--
RR1000 + Si	Wt. %	bal.	18.5	15.0	5.0	3.6	3.0	2.0	0.50	0.06	0.02	0.03	0.5
	At. %	bal.	17.8	16.4	3.0	4.3	6.3	0.63	0.16	0.04	0.14	0.11	1.0

Isothermal Oxidation Testing

Isothermal oxidation testing conducted at the University of Birmingham was performed on samples of FG RR1000, CG RR100 and shot-peened CG RR1000 in laboratory air at 800°C for a period of 200 hours. Prior to testing, samples were ground to remove any residual surface damage before being polished to a 6 μm surface finish. A second batch of specimens was ground to a 1200 grit finish prior to shot-peening. Samples were placed into open alumina boats and inserted into single zone tube furnaces at temperature. The furnaces had been calibrated to +/- 1°C using an N-type thermocouple. Samples were removed from the furnace after 200 hours and allowed to air cool to room temperature.

Isothermal oxidation testing conducted at Cranfield University was performed on samples of FG RR1000 + 0.5 wt.% Si. Samples were machined into ca. 10 mm diameter discs (2 mm thick) and oxidised in laboratory air in open alumina boats at 700°C for 1000 hours. The furnaces had been calibrated to +/- 5°C. Samples were slow-cooled inside the furnace.

Conventional Preparation

Method

Conventional preparation of oxidised specimens for cross-sectional examination is both difficult and time consuming due to the brittle nature of the oxides formed and the potential for introducing

mechanical damage. In order to prevent spallation or cracking of the external oxide layer one of two preparation techniques was used.

1. The sample was mounted in a low shrinkage, low viscosity epoxy resin (Struers Epofix), using a Struers Epovac vacuum impregnator at a pressure of 400 mbar.
2. The sample was first sputtered with gold, to produce an electrically conductive layer (~20 nm thick), then electroplated with Ni (~5 μm layer) using a "Watt's bath" electrolyte ($NiSO_4 \cdot 6H_2O$, $NiCl_2 \cdot 6H_2O$ and H_3BO_3). Ni plating was intended to prevent oxide spallation or damage to the oxide during sectioning. The thin Au layer was used in energy dispersive X-ray (EDX) mapping to delineate the surface of the oxide layer. The specimen was then mounted as in 1 above.

Once mounted as above, normal grinding was undertaken with SiC papers from 240 grit to 4000 grit with water as a lubricant, followed by diamond polishing with final polishing being performed using a Struers MD–Chem cloth with colloidal silica solution. Mounted and polished specimens were cleaned ultrasonically in ethanol before being sputtered with gold to allow scanning electron microscopy (SEM) examination. SEM analysis was performed using a JEOL 7000F FEG SEM with Oxford Instruments EDX software to characterise the oxides formed. The samples prepared for SEM analysis had been previously examined using dual-beam FIB sectioning (see Dual-beam FIB section). This allowed direct comparison of the techniques.

Results

Figure 2 (left-hand column) shows back-scattered electron (BSE) images of three microstructural variants (FG RR1000, CG RR1000 and shot-peened CG RR1000), all without Si, tested and prepared using conventional preparation techniques. It illustrates that there is no evidence for the presence of large voids previously reported [6-8] on sections produced and examined using single-beam FIB. The images in Figure 2 are consistent with previous reports [2-5] of alumina intrusions in the sub-surface zone adjacent to the surface oxide. RR1000 is a complex alloy with a large number of alloying additions which produces a complex oxide scale. EDX analysis (Figure 3) was performed on the conventionally prepared samples and confirmed that the external layer was duplex and rich in Ti, Cr and O with a sub-surface internal network rich in Al and O. These observations correspond well with previous observations that the external oxide is TiO_2 and Cr_2O_3 with an Al_2O_3 internal oxide [2, 3]. At no stage during the preparation method was any colloidal alumina solution used which may have in-filled voids. No polishing media contamination was observed in any of these samples.

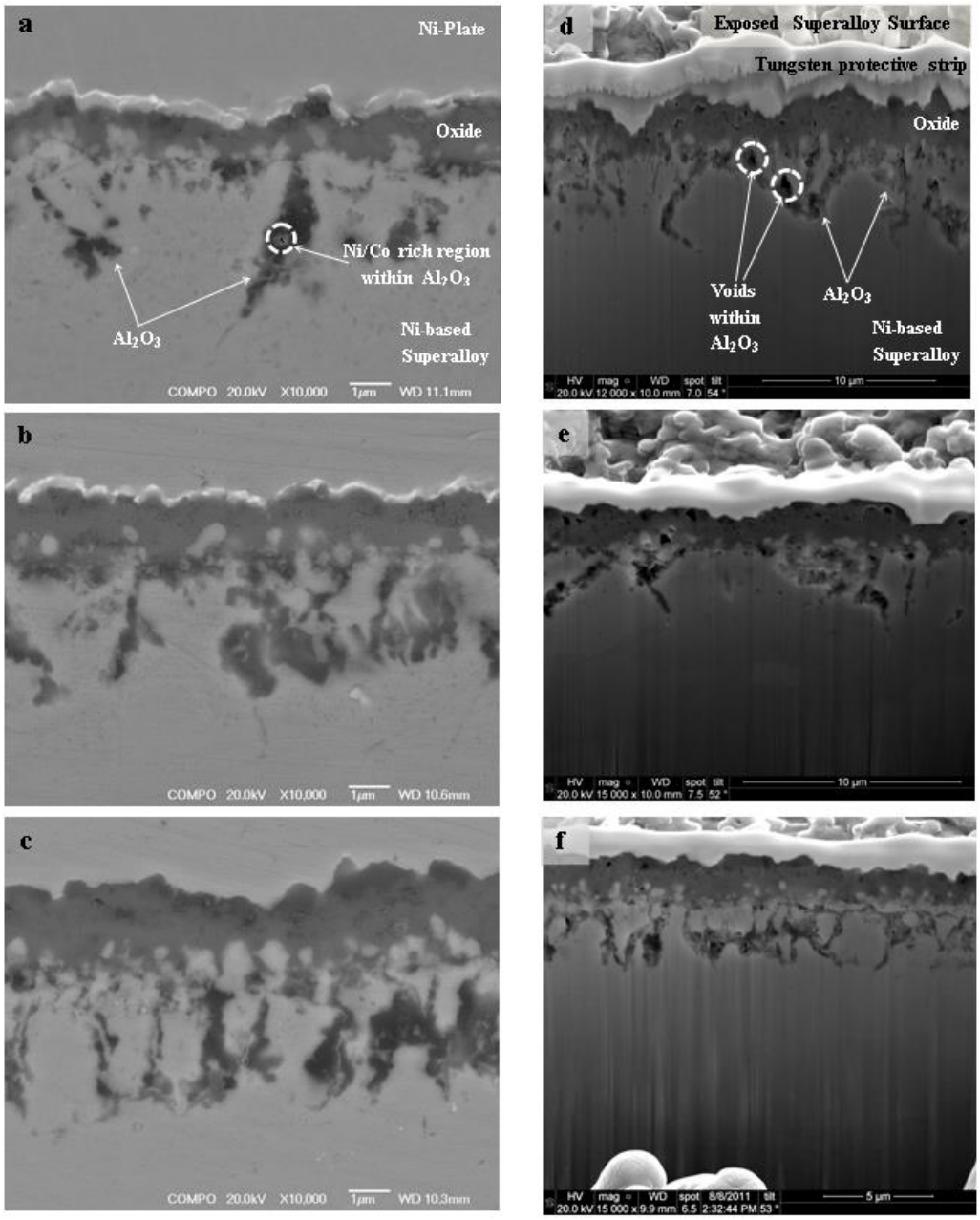

Figure 2. A comparison between a backscattered SEM image of cross-sections prepared using conventional preparation techniques (images on left-hand side) and SEM images, produced using an electron beam ($SE_{electron}$) during FIB sectioning (images on right-hand side) on a) and d) CG RR1000, b) and e) FG RR1000, c) and f) shot-peened CG RR1000.

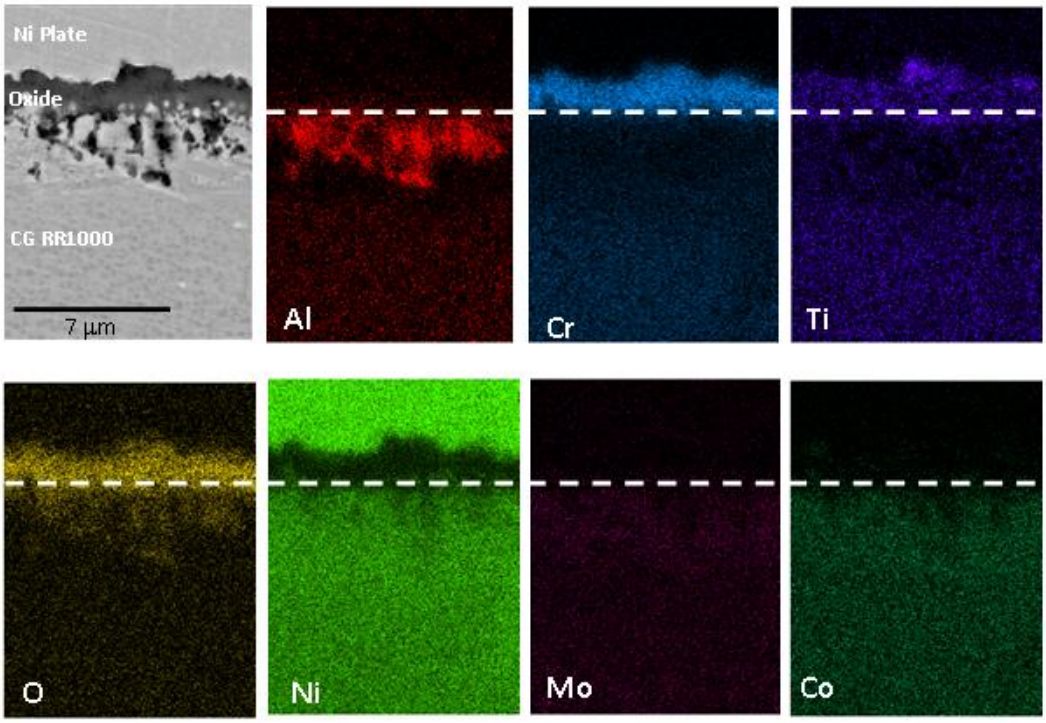

Figure 3. A secondary electron image produced using an electron beam, of a section through a CG RR1000 sample oxidised in laboratory air at 800°C for 200 hours with energy dispersive X-ray analysis maps. White dashed line indicates the interface between the external oxide scale and the alloy.

Dual-Beam FIB Sectioning

FIB Sectioning

Samples of CG RR1000, FG RR1000 and shot-peened CG RR1000 (all without Si), oxidised at 800ºC for 200 hours in laboratory air, underwent dual-beam FIB sectioning at the University of Birmingham using a Quanta 3D dual beam FEG FIB, with a 30 keV gallium ion source, under the conditions listed below.

- The sample was placed on a five-axis motorised stage and tilted to 52° to position the surface perpendicular to the ion beam for milling.
- A protective tungsten layer (~35 x 3 x 2 µm) was deposited on top of the area of interest.
- A trench was milled by a series of gallium ion beams at various currents.
    - First a regular cross section was milled using a 65 nA current.
    - A rectangle was then milled using a 30 nA current.
    - Two clean cross sections were milled using first 7 nA and finally a 1 nA current.
    - This process was repeated with 1 nA (and/or 0.5 nA) current to clean the cross section until the required finish was achieved.

The dual-beam capability allowed the cross-section to be imaged at every stage using the secondary electrons produced by an electron beam ($SE_{electron}$)[1], without moving the sample (Figure 4a).

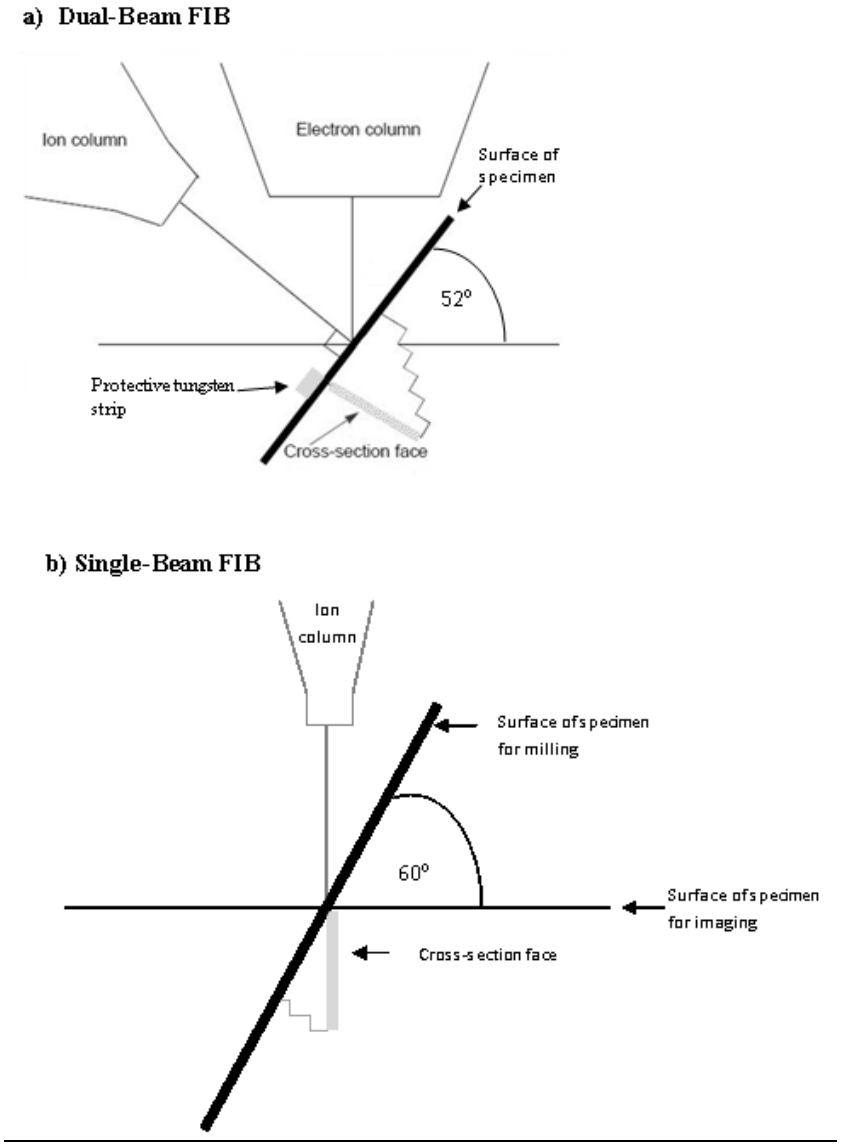

Figure 4. Schematic diagrams of how the sectioning was achieved by a) dual-beam (adapted from [15] and b) single-beam FIB microscopy.

Results

The SEM images of the FIB sections (right hand side, Figure 2) clearly show similar sub-surface structures found in conventional preparation (left hand side). The appearance of these structures is essentially identical to those shown earlier, Figure 1, but in that case they were incorrectly interpreted as voids [6-8]. EDX mapping, Figure 3, identifies these intrusions as alumina, in agreement with earlier work on similar and related alloys [2-3, 5].

[1] $SE_{electron}$ – Secondary electrons produced by the impact of electrons from FEG

It is also worth noting that the interface between the oxide scale and the underlying alloy is similar between the two preparation and imaging methods and shows no evidence of cracking. In both preparation techniques, small voids were present in the outer oxide. The only significant difference between samples produced by the two sectioning techniques is the presence of small void-like features associated with the alumina internal oxide in the FIB specimens (Figure 2(d)). These voids are not the features discussed above, since they are associated with alumina internal oxide and do not change contrast with sample tilt angle.

Returning to Figure 2(a) it was found using EDX that small regions (circled), rich in Co and Ni existed within some of the alumina regions. These had probably formed from small volumes of alloy that had been selectively oxidised to form alumina and had then become entrapped within the alumina intrusion. It appears that the small voids observed after dual-beam FIB sectioning were associated with these metallic regions. The origin of these voids is unclear but may be associated with differential sputtering rates between the metallic and adjacent oxide phases.

Single-Beam FIB Sectioning and Imaging

FIB Sectioning

In addition to the FIB investigations undertaken at the University of Birmingham, samples of FG RR1000 + 0.5 wt.% Si oxidised in laboratory air at 700°C for 1000 hours underwent examination using a FEI FIB 200-SIMS focussed ion beam (FIB) instrument with a single (Ga^+) beam at Imperial College. A trench, ca. 12 µm wide and with a slope of ca. 60° (Figure 4b), was milled then polished under beam currents falling to 3 nA. Both secondary electron (SE_{ion})[2] images and positive secondary ion (SI)[3] were collected following excitation by the 30 kV, 50 pA Ga^+ primary beam using a channeltron detector. Secondary ion (SI) images and secondary ion mass spectroscopy (SIMS) data were also generated with a separate quadrupole-based SIMS detector set to filter only ^{16}O negative ions. Sample tilt angles are given in the text where relevant.

Results

Making use of the bevelled slope of the trench, a cross-section was obtained through the external oxide, sub-surface layer, and into the bulk FG RR1000 + 0.5 wt.% Si alloy. This slope was imaged using SE_{ion}, SI and SIMS modes of the single-beam FIB (Figure 5). One side of the trench can be seen to the right of the images, while the upper sections of each image show the un-milled surface oxide. Material, re-deposited deeper into the trench after polishing the slope prior to imaging, can be seen to the bottom of the images.

[2] SE_{ion} – Secondary electrons produced using an ion beam

[3] SI – Positive secondary ion images produced using the un-filtered total positive ion yield from the impact of the gallium ions.

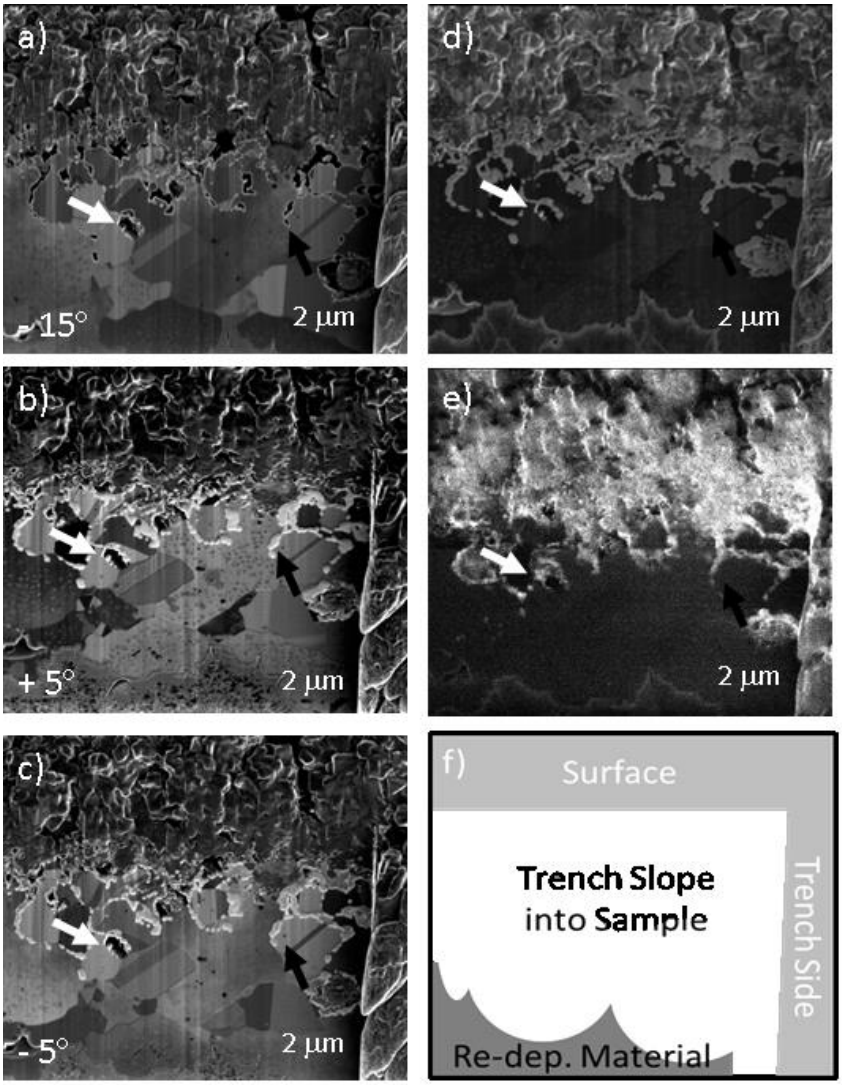

Figure 5. Fine-grained RR1000 + 0.5 wt.% Si sample oxidised for 1000 hours at 700 °C in laboratory air. Ramp milled at ca. 30° to the sample surface. Secondary electron (SE) images, produced using the FIB ion beam, with the sample surface tilted at a) -15°, b) +5° and c) -5°. Note the change in SE contrast with tilt at the black arrows and the constant contrast with tilt at the white arrows. d) Shows a secondary ion (SI) image with the sample surface tilted at +5°. e) ^{16}O negative ions SIMS data. Note that, due to sample tilt, scale is not representative perpendicular to the micron bar. f) Systematic diagram of the trench.

Beneath the surface oxide, there is a region consisting of small grains showing evidence of twinning (Figure 5a) and a network of features can be observed which, under the initial imaging conditions (-15° tilt, SE_{ion} mode, Figure 5(a) are dark contrast (shown by the black arrow). Each of these features is surrounded by a bright ring that may be attributed to edge effects from enhanced secondary electron emission. In Figure 5(a) there are features which strongly resemble voids which have previously been postulated as such [7]. However, as can be seen in Figures 5(b) and 5(c), most of these features change contrast when the sample is tilted relative to the ion beam, black arrow for example, thus showing that these are not voids. This is more obvious in Figure 6 which shows an expanded section

around the black arrow in Figure 5. The intrusion that strongly resembles a void in Figure 6(a) changes contrast with tilt angle (Figure 6(b & c)). In Figure 6(d), the SI image clearly shows it is not a void as does Figure 6(e) that confirms it to be an oxide. The use of tilt when examining samples produced in this way is highly recommended, as demonstrated, as a key technique in identifying features.

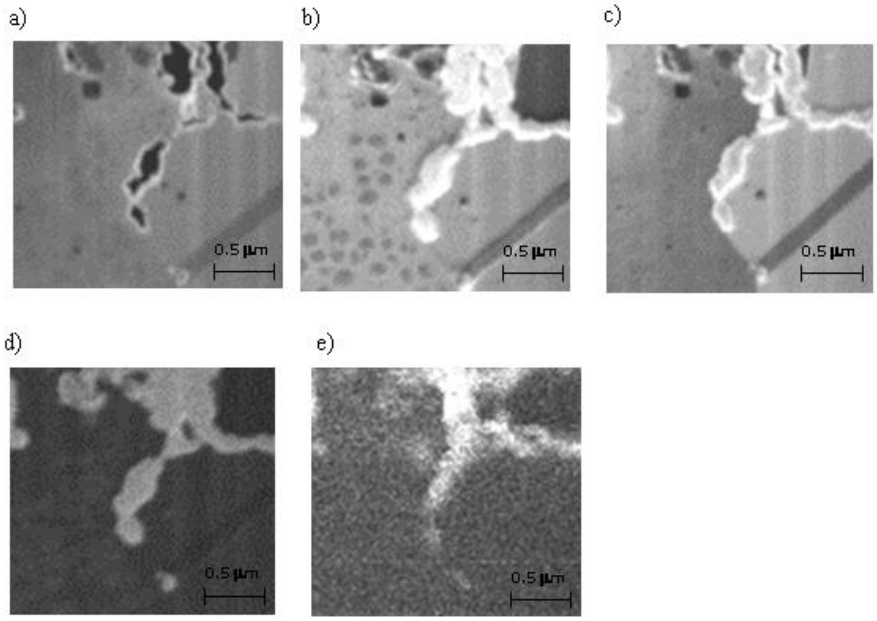

Figure 6. Expanded section of Figure 5(a-e), illustrating more clearly the area highlighted by the black arrow showing the contrast changes with tilt angle and imaging signal. The SE images produced using the FIB ion beam with the sample surface tilted at a) -15º, b) +5º and c) -5º. An SI image of the sample surface tilted at +5º shown in d), with e) ^{16}O negative ions SIMS data.

FIB ion beam sputtered positive secondary ions have a significantly enhanced yield in the presence of oxygen [15] by a factor of approximately 100, which together with the SIMS oxygen negative ion map data, confirm the presence of sub-surface oxides, Figures 5(d) and (e). Not all of the dark features observed in Figure 5(a) change contrast with changing tilt angle or give detectable signals in SI or SIMS mode (white arrow in Figure 5, expanded in Figure 7). Despite this, it has been demonstrated that what was previously termed a network of voids is in fact a network of internal oxides.

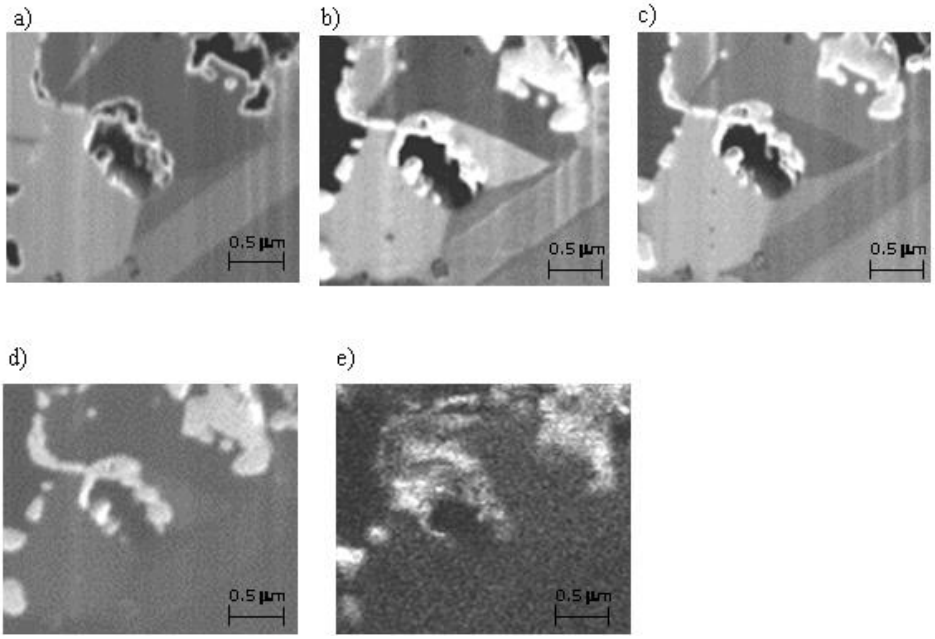

Figure 7. Expanded section of Figure 5(a-e), illustrating more clearly the area highlighted by the white arrow showing the contrast changes with tilt angle and imaging signal. The SE images produced using the FIB ion beam with the sample surface tilted at a) -15º, b) +5º and c) -5º. An SI image of the sample surface tilted at +5º shown in d), with e) ^{16}O negative ions SIMS data.

The examination of a bevelled slope of the trench gives a perspective of the sub-surface structure that shows that the oxide intrusions encircle grains. This is by no means unique to FIB and has been demonstrated also using conventional preparation [3].

Concluding Summary

Conventional sample preparation has shown in the present RR1000 alloys that a solid internal network of alumina is present underneath the external scale rather than a network of voids as suggested elsewhere [6-8]. Features that appear as voids when using SE_{ion} imaging can be established as containing solid matter when a range of tilt angles is used. Detailed explanations as to the mechanisms of channelling contrast can be found in review articles [15, 16] and standard texts [18, 19].

Occasional sub-surface void-type damage can still arise only in the FIB sectioned specimens. Voids of similar size and morphology were absent from the specimen prepared by conventional sectioning methods. The inference is that even well-controlled FIB milling can produce void-like artefacts. In

addition, voids were found in the surface oxide in samples produced by both FIB and conventional preparation techniques.

Nevertheless, FIB sectioning offers significant advantages over conventional techniques. These include the ability to section surface features, e.g. oxides, as well as its usefulness in examining samples from interrupted testing where a surface feature can be sectioned before the sample is returned for further testing. Careful preparation and expertise will always be required however regardless of the preparation and imaging method.

Acknowledgements

The authors acknowledge, with thanks, the financial support provided by the Engineering and Physical Sciences Research Council (ESPRC) and Rolls-Royce plc. for further financial support and the provision of samples.

References

[1] Giggins, C.S., Pettit, F.S. (1971) Oxidation of Ni-Cr-Al alloys between 1000° and 1200°C, *Journal of the Electrochemical Society*, Vol. 118, pp. 1782-1790.

[2] Chen, J., Rogers, P., Little, J. (1997) Oxidation behaviour of several chromia-forming commercial Ni-based superalloys, *Oxidation of Metals*, Vol. 47, pp. 381-410.

[3] Taylor, M.P., Evans, H.E., Stekovic, S., Hardy, M.C. (2011) The oxidation characteristics of the Ni-base superalloy, RR1000, at temperatures 700-900°C in: Microscopy of Oxidation 8, G.J. Tatlock, H.E. Evans (Eds.), Liverpool. Science Reviews 2000 Ltd., pp. 240-245.

[4] Al-hatab, K., Al-bukhaiti, M., Krupp, U., Kantehm, M. (2011) Cyclic oxidation behaviour of IN718 superalloy in air at high temperatures, *Oxidation of Metals*, Vol. 75, pp. 209-228.

[5] Cruchley, S., Taylor, M.P., Evans, H.E., Bowen, P., Hardy, M.C., Stekovic, S. (2012) Microstructural characterisation of high temperature oxidation of Ni-base superalloy, RR1000 and the effect of shot-peening, in: Superalloys 2012: 12th International Symposium on Superalloys TMS, Seven Springs, PA, pp. 751-758.

[6] Encinas-Oropesa, A., Drew, G.L., Hardy, M.C., Leggett, A.J., Nicholls, J.R., Simms, N.J. (2008) Effects of oxidation and hot corrosion in a Ni disc alloy, in: Superalloys 2008: 11th International Symposium on Superalloys TMS, pp. 609-618.

[7] Encinas-Oropesa, A., Simms, N.J., Nicholls, J.R., Drew, G.L., Leggett, J., Hardy, M.C. (2009) Evaluation of oxidation related damage caused to a gas turbine disc alloy between 700 and 800°C, *Materials at High Temperatures*, Vol. 26, pp. 241-249.

[8] Karabela, A., Zhao, L.G., Tong, J., Simms, N.J., Nicholls, J.R., Hardy, M.C., (2011) Effect of cyclic stress and temperature on oxidation damage of a Ni-based superalloy, *Materials Science and Engineering: A*, Vol. 528, pp. 6194-6202.

[9] Engell, H., Wever, F. (1957) Über einige grundfragen der bildung und der haftung von zunder auf eisen, *Acta Metallurgica*, Vol. 5**,** pp. 695-702.

[10] Evans, H.E., Hilton, D.A., Holm, R.A. (1977) Internal attack during the oxidation of nitrided stainless steel, *Oxidation of Metals*, Vol. 11**,** pp. 1-21.

[11] Gorman, A., Higginson, R.L., Du, H., McClovin, G., Fry, A.T., Thomson, R.C. (2012) Microstructural analysis of IN617 and IN625 oxidised in the presence of steam for use in ultra-supercritical power plant, in: 8th International Symposium on High-Temperature Corrosion and Protection of Materials Les Embiez, France.

[12] Bricknell, R.H., Woodford, D.A. (1982) The mechanism of cavity formation during high temperature oxidation of nickel, *Acta Metallurgica*, Vol. 30, pp. 257-264.

[13] Dyson, B.F. (1982) An analysis of carbon/oxygen gas bubble formation in some nickel alloys, *Acta Metallurgica*, Vol. 30, pp. 1639-1646.

[14] Evans, H.E. (1988) Spallation of oxide from stainless steel AGR nuclear fuel cladding: Mechanisms and consequences, *Materials Science and Technology*, Vol. 4, pp. 414-420.

[15] FEI Company (2008), Quanta 3D FEG User Operation Manual.

[16] Munroe, P.R. (2009) The application of focused ion beam microscopy to the material sciences, *Materials Characterization*, Vol. 60, pp. 2-13.

[17] Phaneuf, M.W. (1999) Applications of focused ion beam microscopy to materials science specimens, *Micron*, Vol. 30, pp. 277-288.

[18] Giannuzzi, L.A., Stevie, F. A., (2005) Introduction to focused ion beams: Instrumentation, Theory, Techniques and Practice, Springer.

[19] Orloff, J. (2008) Handbook of charged particle optics, CRC Press.